Phys. Status Solidi B **246**, No. 3, 589–593 (2009) / **DOI** 10.1002/pssb.200880541

physica status solidi b
www.pss-b.com
basic solid state physics

Configuration dependence of the electronic structure and optical properties of BC_2N alloys

Shiyou Chen[1], X. G. Gong[1], and Su-Huai Wei[*,2]

[1] Surface Science Laboratory (National Key) and Physics Department, Fudan University, Shanghai 200433, P.R. China
[2] National Renewable Energy Laboratory, Golden, CO 80401, USA

Received 25 June 2008, revised 12 September 2008, accepted 19 September 2008
Published online 10 December 2008

PACS 61.50.Ah, 62.20.De, 71.20.Nr, 78.40.Fy

[*] Corresponding author: e-mail swei@nrel.gov

Using the first-principles band structure and total energy method, we have studied the general trend of physical properties of the BC_2N alloy as a function of atomic configurations. We found that the mechanical properties of the BC_2N alloy are basically determined by the bond components: structures with more C–C and B–N bonds have low energy, high density, and high bulk and shear moduli, which validates the so called the bond counting rule. We also show that the electronic and optical properties of the BC_2N alloy are more sensitive to the atomic configuration, thus could be used in future experimental measurement to identify the atomic configuration of BC_2N samples. A strong internal electric field produced by the polar interfaces is observed in the long period $BC_2N_{n\times n}$ (111) superlattices, which explains the significant band gap decrease as the period n increases.

1 Introduction Cubic (c) BC_2N alloys of diamond and c-BN are expected to be thermally and chemically more stable than diamond and harder than c-BN, thus, they have been extensively studied both theoretically and experimentally during the last twenty years [1, 2]. Several groups have synthesized BC_2N samples from different starting materials and using different methods under high temperature and high pressure [3]. Among these experiments, the BC_2N samples obtained by Knittle et al. [4], Utsumi et al. [5], Zhao et al. [6] have lattice constants between 3.595 Å and 3.602 Å, which are close to the ideal averaged value of diamond (3.567 Å) and c-BN (3.616 Å), whereas the one obtained by Solozhenko et al. is larger at 3.642 Å [7]. From the direct measurement of the hardness, Zhao et al. showed that high density samples have ultrahigh hardness, second only to diamond [3]. The low density sample was found to have relatively small bulk modulus (259 GPa) and shear modulus (238 GPa) [7], which suggests that the material may easily be compressed and deformed. However, unexpectedly, the hardness measurement of Solozhenko et al. showed that the low density samples also have ultrahigh hardness [3]. X-ray diffraction peaks showed that the BC_2N alloys crystallize in the diamond-like cubic structure, however, the exact atomic configurations in the diamond-like structure is unknown.

Dozens of papers have been devoted to the theoretical study of the crystal structure and mechanical properties of BC_2N. In most cases, several atomic configurations were considered and the total energy, lattice constant, bulk modulus, and shear modulus were calculated and compared with experimental data, trying to identify the ones that have physical properties similar to the experimental samples. For example, seven topologically different configurations of BC_2N-m (m = 1–7) within an eight-atom cubic diamond-like unit cell were identified by Sun et al. [8]. Based on the calculations using the local density approximation (LDA) to the density functional theory, low energy BC_2N-1 (also denoted as β-BC_2N [9], which is a (010) BN/C_2 superlattice, see Fig. 1(b)) and BC_2N-2 were assigned to the high density samples, whereas high energy BC_2N-5 and BC_2N-6 were assigned to low density samples because the calculated lattice constants and bulk moduli are close to the experimental values. However, recent calculations using the generalized gradient approximation

(GGA) performed by Kim et al. [10] obtained larger lattice constants and smaller bulk moduli for BC_2N-m and suggested that BC_2N-3 structure corresponds to the low density samples. However, these calculations neglected the fact that B, C, and N atoms can have many other configurations on the diamond lattice sites, therefore BC_2N alloys can have many other unit cells with different shapes and sizes such as the tetragonal chalcopyrite (ch) BC_2N (Fig. 1(c)). All the coherent BC_2N alloys are expected to have similar lattice constants within the range of experimental values [3, 11]. Therefore it is not very reliable to assign certain configurations to the experimental structures by simply comparing the lattice constants or bulk modulus due to the uncertainty in LDA and GGA.

Besides the bulk and shear modulus calculation, empirical formulae were also proposed by Gao et al. [12], Šimunek et al. [13], and Li et al. [14] to predict the Vickers or Knoop hardness of materials based on the bond length, charge density, ionicity, electronegativity, or other properties at equilibrium volume. Applying these formulae to different BC_2N configurations, BC_2N-1 and ch-BC_2N were shown to have large Vickers hardness, 78 GPa [12] and 72.2 GPa [11], respectively, both close to the experimental values (76 ± 4 GPa) of the low density samples [7]. However, it should be noted that the Vickers or Knoop hardness measured by different groups could be very different for the same material depending on the sample quality and the measurement techniques. For example, the measured Vickers hardness of diamond is 115 GPa in Ref. [7], whereas 85 GPa was given in Ref. [6] and 90 GPa was cited in Ref. [12]. Therefore, identifying BC_2N crystal atomic configuration by comparing the calculated hardness values using formulae fitted to the hardness values of other materials measured by different groups could be misleading.

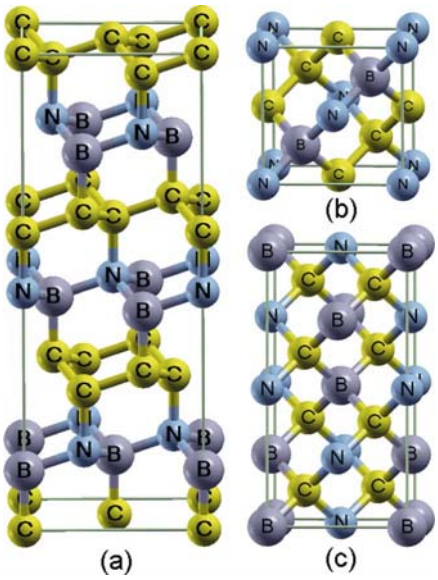

Figure 1 (online colour at: www.pss-b.com) Crystal structures of (a) $BC_2N_{1\times1}$, a BN/C_2 1×1 (111) superlattice. The lattice vectors of a primitive cell are $a_1 = \langle -0.5, 0, 0.5\rangle$, $a_2 = \langle 0, -0.5, 0.5\rangle$ and $a_3 = \langle 1, 1, 0\rangle$ with R3m space group; (b) BC_2N-1, a (010) superlattice; and (c) ch-BC_2N, a (201) superlattice.

In our investigation, we have adopted a different approach to studying the physical properties of BC_2N alloys. Rather than calculating the properties of a few BC_2N configurations, we studied the general trend of physical properties as a function of atomic configurations. We found that the mechanical properties of the BC_2N alloy are basically determined by the bond components: structures with more C–C and B–N bonds have low energy, high density, and high bulk and shear moduli, whereas those with B–B and N–N bonds have higher energy, lower density, and low elastic moduli, which validates the "bond counting rule" [3]. By performing a unit-cell-shape unconstrained search, we have identified a series of small-cell c-BN/C_2 alloys, which are BN/C_2 (111) superlattices [denoted as $BC_2N_{n\times n}$ with $n = 1, 2, 3$, etc., see Fig. 1(a)], that maximize the number of C–C and B–N bonds with a given primitive cell size [15]. These superlattices are energetically much more stable than any of the BC_2N-m [8, 16] and ch-BC_2N structures and also have larger bulk and shear moduli. By calculating the ideal strength (IS) [15, 16] and ideal shear strength under normal compression (ISSNC) [3], we found that these low-energy structures have higher IS and ISSNC than that of c-BN. We propose that these (111) superlattice BC_2N and similarly BC_4N may have higher hardness than c-BN, because the large bulk and shear modulus indicate they are strong in resistance to volume compression and deformation, while the large IS and ISSNC indicate the crystals are also strong to plastic deformation under nanoindentation. In this paper, we also calculate the electronic structure and optical properties of a series of BC_2N alloys with configurations containing different C–C and B–N bond components. We show that these electronic and optical properties are more sensitive to the atomic configuration, thus could be used in future experimental measurements to identify atomic configuration of BC_2N samples.

2 Methods of calculations The total-energy and stress calculations are carried out using density functional theory as implemented in the ABINIT code [17] that is based on pseudopotential and planewave basis functions. The norm-conserving Troullier–Martins pseudopotential [18] is used with the cutoff radii of 1.59, 1.49, and 1.50 a.u. for B, C, and N, respectively. We use the LDA and the exchange–correlation functional of Perdew–Wang as parameterized by Teter [19]. For the Brillouin-zone integration, we used an $8 \times 8 \times 8$ Monkhorst–Pack k-point grid for an eight-atom cubic unit cell and equivalent k-points for other structures. The cut-off energy for the basis function is 80 Ry. Our convergence test of k-points and energy cutoff show that the uncertainty in the calculated stress values is less than 0.1 GPa. The core levels of the B, C, and N atoms in BC_2N are calculated using the VASP package where the interaction between the core and valence electrons is included by

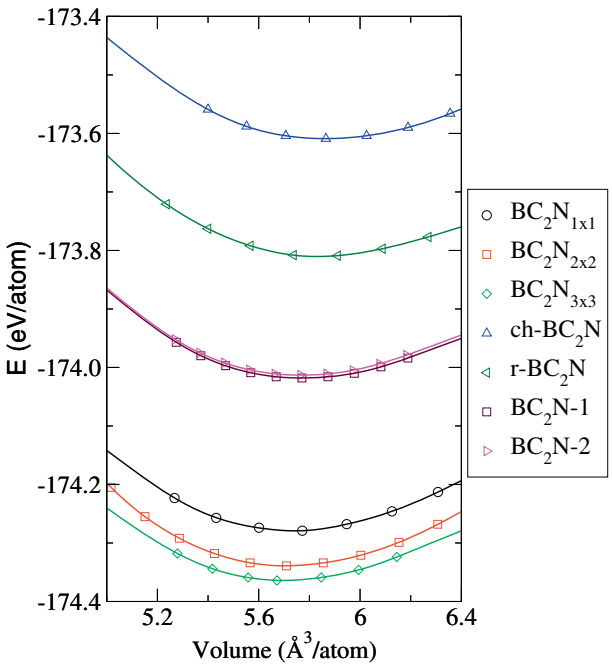

Figure 2 Calculated energy dependence on the volume of different BC_2N structures.

the standard frozen-core projector augmented-wave potentials.

3 Results and discussions

3.1 Ground state and elastic properties Table 1 summarizes our calculated properties of seven BC_2N structures without unstable B–B and N–N bonds, as well as diamond, c-BN, and $BC_4N_{2\times1}$. A bond-component parameter η is defined to describe the fraction of the ideal C–C and B–N bonds relative to the total number of the bonds:

$$\eta = \frac{n_{C-C} + n_{B-N}}{n_{C-C} + n_{B-N} + n_{C-B} + n_{C-N}} \quad (1)$$

where n stands for the number of a specific bond in the structure. The seven BC_2N structures are selected to cover η from 0 to about 1. As we can see, in $BC_2N_{n\times n}$ the C–N and C–B bonds exist only at the interface along the (111) direction (Fig. 1(a)), hence $\eta = 1 - 1/4n$. BC_2N-1, BC_2N-2, r-BC_2N (see Fig. 1(b) in Ref. [3]) and ch-BC_2N have smaller η, and $\eta = 0$ for ch-BC_2N, which has no C–C and B–N bond (Fig. 1(c)). Our calculations for these diamond-like BC_2N configurations found that their structure factors are similar to each other and the (200) peak, which reflects the difference between the atoms on the two fcc-sublattices and are always weak due to the close atomic number of B, C, and N. Therefore, it will also be difficult to use the structure factors to determine the atomic configuration in this system.

Our calculated results show that as η increases, the formation energy [3] ΔE decreases drastically from 3.41 eV/4-atoms for ch-BC_2N to 0.39 eV/4-atoms for $BC_2N_{3\times3}$, indicating that high energy ch-BC_2N is energetically impossible to form. The lattice constants and bulk moduli also show a monotonic decrease as the number of C–C and B–N bonds decrease, indicating that structures with more C–C and B–N bonds are denser and stronger in resistance to volume compression. The formation energy and volume dependence on η are almost linear, as can be seen in Table 1 and Fig. 2. For example, the energy vs. volume curves of BC_2N-1 and BC_2N-2 ($\eta = 0.5$) fall just in the middle of those of ch-BC_2N ($\eta = 0$) and $BC_2N_{3\times3}$ ($\eta = 0.967$, close to 1). The minima of the curves also move to the right side slightly from $BC_2N_{3\times3}$ to ch-BC_2N. Among all these BC_2N structures studied here, $BC_2N_{n\times n}$ exhibit not only the lowest energy and volume, but also largest bulk modulus and shear modulus [3].

3.2 Band structure and optical properties Results in Table 1 and Fig. 2 also show that configurations with the same bond component are nearly degenerate in the values of lattice constant or bulk modulus. The variation of the lattice constants as a function of the bond component

Table 1 LDA calculated alloy formation energy ΔE per 4-atoms, lattice constants a_0, bulk moduli B_0, pressure derivative of bulk modulus B', isotropic shear moduli G, and the fundamental band gap E_g for diamond, c-BN, $BC_4N_{2\times1}$, and BC_2N structures studied in this paper as a function of bond-component parameter η. The LDA band gap error is estimated to be 1.5 eV for the BC_2N alloys.

	η	ΔE (eV)	a_0 (Å)	B_0 (GPa)	B'	G (GPa)	E_g (eV)
diamond	1	...	3.542	454	3.56	539(547[8])	4.20
c-BN	1	...	3.593	392	3.81	405(407[8])	4.37
$BC_2N_{3\times3}$	0.967	0.39	3.573	422	3.53	449	2.76
$BC_2N_{2\times2}$	0.875	0.52	3.575	420	3.33	458	3.74
$BC_2N_{1\times1}$	0.750	0.76	3.579	420	3.70	458	3.87
BC_2N-1	0.500	1.78	3.586	398	3.15	431[8]	1.63
BC_2N-2	0.500	1.80	3.586	400	3.71	422[8]	2.09
r-BC_2N	0.250	2.62	3.602	382	3.20	–	1.45
ch-BC_2N	0.000	3.41	3.607	377	4.06	436[11]	3.15
$BC_4N_{2\times1}$	0.833	0.57	3.567	428	3.39	481	3.96

is also very small. So it is desirable to use other physical properties to distinguish different BC_2N alloy configurations. In this aspect, electronic structure and optical properties are good quantities for the structural characterization, because they are more sensitive to the atomic configuration than lattice constant, bulk modulus, and shear modulus and are easier to measure. In the following, we will discuss in detail the band gap, density of states, and optical dielectric function of the BC_2N alloys as a function of its configurations, which can be compared with future experimental measurements.

Table 1 shows the LDA calculated band gaps of the BC_2N alloy in various configurations. It is well known that LDA underestimates the band gap (estimated to be about 1.5 eV for BC_2N), but the difference between the band gap for compounds at fixed composition is usually correctly reproduced due to the cancellation of the band gap error. We find that although the variation of the lattice constants is small for all the studied BC_2N alloys, the variation for the band gap is large, from 3.87 eV for $BC_2N_{1\times1}$ to 1.45 eV for r-BC_2N. This is true even for structures with the same η. For example, the difference of the band gap between BC_2N-1 and BC_2N-2, both with $\eta = 0.5$, is 0.45 eV. This is because for different structures, the coupling potential between k-points in the diamond Brillouin zone are different even when they have the same η. It indicates that measuring the band gap could be an efficient approach to distinguish different structures.

Figure 3 gives the total density of states (DOS) of ch-BC_2N ($\eta = 0$), BC_2N-1 ($\eta = 0.5$), and $BC_2N_{1\times1}$ ($\eta = 0.75$). We see that, besides the difference in their band gaps, the detailed features of the DOS are also different. For example, ch-BC_2N has an intervalence band gap at about 17 eV below the VBM. However, the general features of the DOS are similar. From the partial DOS projected on atoms, we see that the upper valence band is mainly the bonding p component of B, C, and N, whereas the bottom of the conduction band has a mostly antibonding p component of B, C and N.

Figure 4 plots the real part ε_1 and imaginary part ε_2 of the optical dielectric functions for ch-BC_2N, BC_2N-1, and $BC_2N_{1\times1}$, from which the refractive index, adsorption coefficient, reflectivity, and electron energy-loss spectrum can be deduced. According to the symmetry of ch-BC_2N and $BC_2N_{1\times1}$, the optical axes are along the (001) and (111) directions, respectively. For BC_2N-1, we consider polarizations both perpendicular and parallel to the superlattice direction (010). The overall shapes of the three ε_2 curves for the three structures are similar to that of the diamond, indicating the structural and chemical bond similarity to diamond. For ε_2 of ch-BC_2N, there are two peaks near 9 eV for both polarizations, which correspond to the interband transitions from valence state near –3.1 eV and –1.6 eV to the conduction state near 6.2 eV and 7.2 eV (Fig. 3). The band edge optical transition is very weak, because the system is essentially indirect and the conduction band edge has mostly atomic p characters. ε_2 starts to increase at about 5 eV when the conduction states contain significant s character. The threshold is lower for BC_2N-1, which has a quite small band gap (1.63 eV). However, ε_2 for BC_2N-1 is more isotropic; there are no obvious separate peaks in ε_2 for different polarizations. For ε_2 of $BC_2N_{1\times1}$, the peaks for the two polarizations shifts a little: the left one (11.2 eV) of the polarization along (111) corresponds to the transition from the valence state at –3.4 eV to the conduction state at 7.9 eV, and the right one (11.5 eV) of the polarization perpendicular to (111) corresponds to the transition from the valence state at –3.7 eV to the conduction state at 7.9 eV.

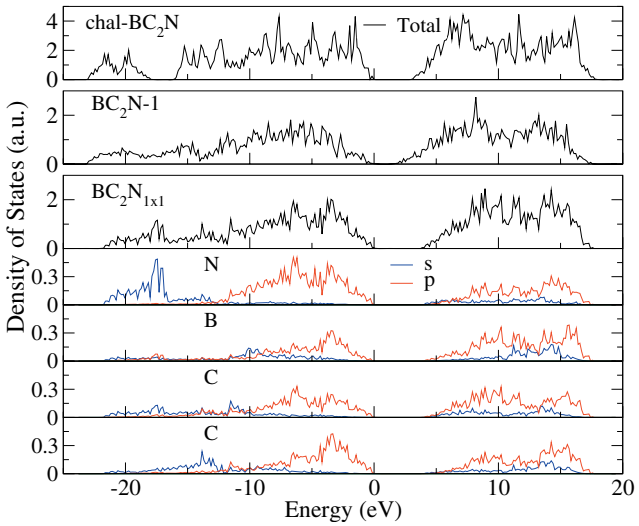

Figure 3 Total density of states of ch-BC_2N, BC_2N-1 and $BC_2N_{1\times1}$ and the partial density of states projected on four inequivalent B, C, and N atoms in $BC_2N_{1\times1}$.

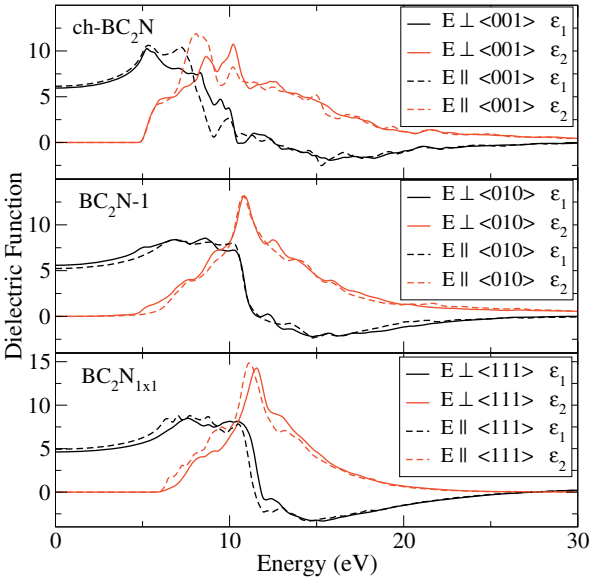

Figure 4 LDA calculated real part ε_1 and imaginary part ε_2 of the optical dielectric function of ch-BC_2N, BC_2N-1, and $BC_2N_{1\times1}$ with both polarizations.

It is interesting to notice that for $BC_2N_{n\times n}$ ($\eta = 1-1/4n$), the calculated band gap decreases on the order of 3.87, 3.74, 2.76, 1.51, and 0.16 eV for $n = 1-5$ and becomes metallic at $n = 6$. This monotonic decrease of the band gap can be traced to the internal electric field directed from the C–B interface to the C–N interface, as reflected in the core level shifts (see Fig. 5) in these superlattice structures. As we know, the C–N bond is more electronegative than the C–B bond, so there is electron charge transfer from the C–B bonds to the C–N bonds at the (111) interfaces. This creates an electric field between the two interfaces [20], decreasing the band gap. As the period becomes longer, the field, which is determined by the charge at the interface, is nearly constant, but the potential drop becomes larger between the two interfaces, making the band gap smaller. The effect of the potential drop on the 1s core levels of the B, C, and N at different positions between the interfaces for $BC_2N_{5\times5}$ is plotted in Fig. 5. As we can see, the core level shift could be very large (as large as 7 eV for N 1s core level in $BC_2N_{5\times5}$), indicating that the internal electric field is very strong. Eventually, when the energy of the valence band maximum, which is more localized near the C–B interface, is higher than the energy of the conduction band minimum, which is more localized near the C–N interface, the band gap closes and the system becomes metallic. The internal electrical field caused by the polar interfaces and the band gap reduction have also been seen in $(Si_2)_n(GaP)_n$, $(Ge_2)_n(GaAs)_n$, and $(Si_2)_n(GaAs)_n$ (111) superlattices [21], and it has been shown that structural reconstruction at the interface can occur to remove the polarity and the field [22].

4 Summary In conclusion, using first-principles calculation, we studied the mechanical properties, electronic structures, and optical properties of a series of BC_2N structural configurations with different bond components. Relative to the lattice constant and bulk or shear modulus, the band gap, density of states, and optical properties are more sensitive to the atomic configuration, which can be used more effectively as the properties for the crystal structure characterization. We also showed that there is a strong internal electrical field between the C–N and C–B interfaces of the $BC_2N_{n\times n}$ (111) superlattice, which decreases the band gap as its period increases.

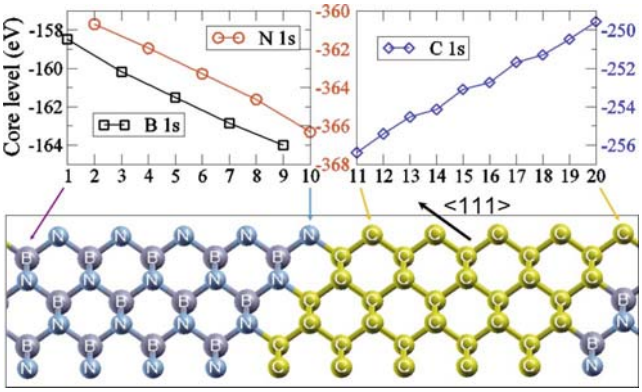

Figure 5 (online colour at: www.pss-b.com) B, N, and C 1s core level dependence on the atomic position in the $BC_2N_{5\times5}$ (111) superlattice.

Acknowledgements The work at Fudan University is partially supported by the National Science Foundation of China, the Special Funds for Major State Basic Research, and the Shanghai Project. The computation is performed in the Supercomputer Center of Shanghai, the Supercomputer Center of Fudan University, and CCS. The work at NREL is funded by the U.S. Department of Energy, under Contract No. DE-AC36-99GO10337.

References

[1] D. M. Teter, Mater. Res. Bull. **23**, 22 (1998).
[2] R. B. Kaner, J. J. Gilman, and S. H. Tolbert, Science **308**, 1268 (2005).
[3] S. Chen, X. G. Gong, and S.-H. Wei, Phys. Rev. B **77**, 014113 (2008), and references therein.
[4] E. Knittle, R. B. Kaner, R. Jeanloz, and M. L. Cohen, Phys. Rev. B **51**, 12149 (1995).
[5] W. Utsumi, S. Nakano, K. Kimoto, T. Okada, M. Isshiki, T. Taniguchi, K. Funakoshi, M. Akaishi, and O. Shimomura, Proceedings of AIRAPT-18, Beijing, China (2001), p. 186.
[6] Y. Zhao et al., J. Mater. Res. **17**, 3139 (2002).
[7] V. L. Solozhenko, D. Andrault, G. Fiquet, M. Mezouar, and D. C. Rubie, Appl. Phys. Lett. **78**, 1385 (2001).
[8] H. Sun, S. H. Jhi, D. Roundy, M. L. Cohen, and S. G. Louie, Phys. Rev. B **64**, 094108 (2001).
[9] R. Q. Zhang, K. S. Chan, H. F. Cheung, and S. T. Lee, Appl. Phys. Lett. **75**, 2259 (1999).
[10] E. Kim, T. Pang, W. Utsumi, V. L. Solozhenko, and Y. Zhao, Phys. Rev. B **75**, 184115 (2007).
[11] J. Sun, X. F. Zhou, G. R. Qian, J. Chen, Y. X. Fan, H. T. Wang, X. Guo, J. He, Z. Liu, and Y. Tian, Appl. Phys. Lett. **89**, 151911 (2006).
[12] F. Gao, J. He, E. Wu, S. Lu, D. Yu, D. Li, S. Zhang, and Y. Tian, Phys. Rev. Lett. **91**, 015502 (2003).
[13] A. Šimunek and J. Vackář, Phys. Rev. Lett. **96**, 085501 (2006).
[14] K. Li, X. Wang, F. Zhang, and D. Xue, Phys. Rev. Lett. **100**, 235504 (2008).
[15] S. Chen, X. G. Gong, and S.-H. Wei, Phys. Rev. Lett. **98**, 015502 (2007).
[16] Y. Zhang, H. Sun, and C. Chen, Phys. Rev. Lett. **93**, 195504 (2004).
[17] X. Gonze et al., Z. Kristallogr. **220**, 558 (2005).
[18] N. Troullier and J. L. Martins, Phys. Rev. B **43**, 1993 (1991).
[19] S. Goedecker, M. Teter, and J. Hutter, Phys. Rev. B **54**, 1703 (1996).
[20] W. A. Harrison, E. A. Kraut, J. R. Waldrop, and R. W. Grant, Phys. Rev. B **18**, 4402 (1978).
[21] R. G. Dandrea, S. Froyen, and A. Zunger, Phys. Rev. B **42**, 3213 (1990).
[22] R. M. Martin, J. Vac. Sci. Technol. **17**, 978 (1980).